Journal of the Korean Electrochemical Society
Vol. 28, No. 1, 2025, 14-23
https://doi.org/10.5229/JKES.2025.28.1.14

Research Paper
pISSN 1229-1935
eISSN 2288-9000

Water-enriched WO_3 Nanostructures for Electrochromic Energy Storage and Photovoltaic Cell Integrated Electrochromic System

Aryal Krishna Prasad and Kwang-Soon Ahn*

School of Chemical Engineering, Yeungnam University, Gyeongsan 712-749, South Korea

(Received October 28, 2024 : Revised December 18, 2024 : Accepted January 21, 2025)

Abstract : Water-enriched tungsten oxide (We-WO_3), synthesized via extended ultrasonication and electrochemical deposition, showed multifunctionality in electrochromic (EC) device and energy storage system. As an EC film, it achieved 73.6% optical contrast, 3.3 s coloration time, and 93.1 cm^2/C coloration efficiency. Meanwhile, We-WO_3 exhibited a charge transfer resistance of 20.5 Ω, a reasonable capacitance of 35.6 mF/cm^2, and capacitance retention of 78.4%. Water enrichment improved particle dispersion, altered its morphology, and intensified the Li^+ ion activity. Integrated with a quantum-dot-sensitized solar cell (QDSSC), the We-WO_3 EC film functioned effectively without an external power source using the QDSSC's 0.56 V open-circuit voltage.

Keywords : Tungsten oxide, Water-enrichment, Electrochromic device, Energy storage, Quantum dot-sensitized solar cell

1. Introduction

Advancements in modern technologies in the electrochromic (EC) energy device sector have garnered a significant attention. Continuous improvements in energy consumption sources have led to the widespread development of EC displays. The crucial features of EC devices include their ability to maintain indoor–outdoor temperatures and their eye-friendly nature during use. The underlying working principle of EC films is rooted in their redox reactions. Traditionally, EC devices rely on external power supplies for their operation. However, issues such as response lag during light modulation with an external source have prompted the exploration of alternative power sources, with photovoltaic (PV) cells emerging as viable options for powering EC devices.[1–4)]

WO_3 stands out as a versatile material for EC applications, serving as a component of both EC devices[5–10)] and energy storage[11–14)] for several years. Despite considerable achievements using WO_3, challenges such as insufficient optical modulation and poor diffusion coefficients persist. Numerous studies have been conducted to address these issues. Studies have indicated that the EC properties of WO_3 and its related oxides are highly dependent on the water content. An advantageous correlation between a higher water content and facilitated Li^+ insertion has been observed, which can potentially enable a faster optical response.[15–19)] In this study, the surface of a WO_3 nanostructure is modified using an extended ultrasonication process. The findings reveal that this modification not only augments the water content but also enhances particle dispersion and reactivity, with prospective benefits for improving both EC and energy-storage performance.[15)] The EC performance of the resulting water-enriched WO_3 (We-WO_3) film without external wiring is also investigated. A novel assembly of the integrated device is developed, as shown in Fig. S1, featuring photovoltaic power cells as an alternative energy source. Reports suggest that even PV cells with a small area can provide sufficient power to operate a large EC device, thus showing potential for practical applications.[20,21)]

*E-mail: kstheory@ynu.ac.kr (K.-S. Ahn)
† Electronic Supplementary Information (ESI) available

In this study, a We-WO_3 thin film is meticulously synthesized using an extended ultrasonication method followed by electrochemical deposition (ECD). Both the EC and energy-storage capabilities are evaluated for multifunctional purposes. Additionally, an innovative approach is employed by integrating quantum-dot-sensitized solar cells (QDSSCs) as an alternative power source for an EC device, resulting in the development of a PV-EC system. An integrated setup is designed to explore and analyze the EC performance of We-WO_3 in the absence of an external power source.

2. Experimental

2.1 Materials

Diverse chemical reagents, including sodium tungstate dihydrate, sodium sulfide anhydrate, nitric oxide, boric acid, cadmium nitrate tetrahydrate, selenium dioxide, sodium borohydride, zinc nitrate hexahydrate, copper nitrate pentahydrate, and hydrogen peroxide, were procured from Sigma-Aldrich. Solvents (poly-pyrrole carbonate (PC), ethanol, methanol, and acetone) were sourced from Daejung (Korea).

2.2 Synthesis of WO_3 and We-WO_3 EC films

Thin films of WO_3 and We-WO_3 were fabricated on the surface of indium-doped tin oxide (ITO). In the deposition of WO_3, a constant potential of -0.8 V was applied for 100 s using a three-electrode cell system[4,8], as confirmed by linear sweep voltammetry measurement (Fig. S2). The system comprised an indium tin oxide (ITO) substrate (resistivity = 8 Ω/sq) as the working electrode, Pt wire as the counter electrode, and Ag/AgCl as the reference electrode. An aqueous solution of 0.1 M $Na_2WO_4{\cdot}2H_2O$ adjusted to pH 1.0 was used as the deposition solution. To prepare the We-WO_3, a 0.1 M $Na_2WO_4{\cdot}2H_2O$ solution was ultrasonicated for 24 h at room temperature and utilized for the deposition of the We-WO_3 by applying the same potential of -0.8 V. These processes resulted in the fabrication of WO_3 and We-WO_3 films.

2.3 Preparation of TiO_2 ionic layer and Cu_2S counter electrode on same substrate

To fabricate an ionic storage layer for EC cells, a coating of TiO_2 (Ti-Nanoxide T/SP, Solaronix SA) was applied at one end of the ITO substrate using the doctor blade method.[21,22] The coated layer of TiO_2 was subsequently dried and sintered at 450 °C for 30 min. Simultaneously, a Cu_2S counter electrode for the QDSSC was prepared at the opposite end of the same substrate using the electrodeposition method, followed by sulfurization.[4]

2.4 Unique assembly of QDSSC-assisted integrated device

To create a photoanode for the QDSSC, TiO_2 (Ti-Nanoxide T/SP, Solaronix SA) was synthesized on the FTO surface using the doctor blade method. Subsequently, the successive ionic layer adsorption and reaction (SILAR) method was implemented to form CdS and CdSe quantum dot layers, along with a ZnS passivation layer, over the TiO_2 layer. SILAR was performed using the methodology outlined in our previous reports.[22,23] To assemble the integrated device (PV-EC), the TiO_2 ionic layer and Cu_2S counter electrode were combined in a sandwich structure with the prepared We-WO_3 EC film and TiO_2/CdS/CdSe/ZnS photoanodes, respectively. A non-aqueous 1 M $LiClO_4$/propylene carbonate (PC) solution with TiO_2 was used as the electrolyte-sandwiched EC device. On the other hand, a polysulfide comprising 1 M S, 1 M Na_2S, and 0.2 M KCl in methanol/DI water (7:3 by volume) was used as the redox electrolyte for the QDSSC cell.

2.5 Characterization

The morphologies of the as-prepared thin films were analyzed using FE-SEM (S-4800, Hitachi, Japan) at an accelerating voltage of 10 kV and a working distance of 7 mm. The surface was investigated using transmission electron microscopy (TEM), high-resolution TEM (HRTEM), and selected-area electron diffraction (SAED). Elemental mapping of the thin film surface was also performed.

The chemical environments of the synthesized thin films were studied using X-ray photoelectron spectroscopy (XPS). The We-WO_3 was subjected to

thermogravimetric analysis (TGA) and Fourier-transform infrared spectroscopy (FTIR). Its electrochemical performance was evaluated using a three-electrode cell system with $LiClO_4$/PC as the non-aqueous electrolyte solution. To study the optical characteristics, a UV-visible spectrophotometer (Model: S-3100, SCINCO) was used in combination with an electrochemical workstation (IVIUM Technologies, COMPACTSTAT.e) over the wavelength range of 300–900 nm. The optical measurements were performed under xenon illumination.

3. Results and Discussion

3.1 Mechanism of fabrication of WO_3 and We-WO_3

The fabrication of WO_3 involves using a simple ECD method. An aqueous solution of 0.1 M $Na_2WO_4{\cdot}2H_2O$ in H_2O_2 was prepared for the deposition of the WO_3 thin film. The following chemical reactions occurred during the deposition process[8,11]:

$$2W_2O_4^{2-} + 4H_2O_2 \rightarrow W_2O_{11}^{2-} + 2OH^- + 3H_2O \quad (1)$$

$$W_2O_{11}^{2-} + (2 + 2x)\ H^+ + 2xe^- \rightarrow 2WO_3 + (2 + 2x/2)\ H_2O + (8-2x/2)\ O_2 \quad (2)$$

Similarly, an ultrasonicated 0.1 M $Na_2WO_4{\cdot}2H_2O$ solution was employed for the deposition of the We-WO_3 film. For both films, the ECD technique at a constant potential of -0.8 V for 100 s afforded well-deposited WO_3 and We-WO_3 EC films covering the surface of the ITO substrate.

3.2 Physical characteristics

The morphologies of the prepared WO_3 and We-WO_3 thin films are presented in Fig. 1. Fig. 1(a, b) illustrates the dense morphology of the small tungsten ion nanoparticles, which is a common characteristic. In contrast, We-WO_3 exhibited a well-dispersed and exposed morphology, as depicted in Fig. 1(d, e).

The dispersion and exposure of the morphology are attributed to intense ultrasonication for an extensive duration, which may have enhanced the water content of the WO_3 nanostructures. The improved morphology of We-WO_3 is expected to intensify the movement of Li^+ ions, thereby significantly enhancing the electrochemical and optical properties. Cross-sectional SEM images of the WO_3 and We-WO_3 films are displayed in Fig. 1(c, f), respectively. The thickness of the WO_3 and We-WO_3 films was similar at 1.15 μm and 1.12 μm, respectively.

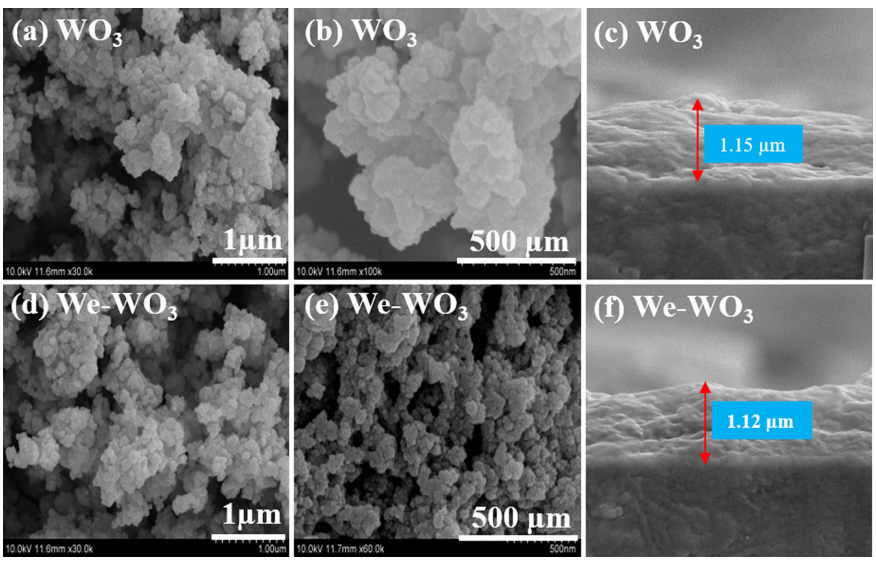

Fig. 1. (a, b) SEM images and (c) cross-sectional image of WO_3; (d, e) SEM images and (f) corresponding cross-sectional image of We-WO_3.

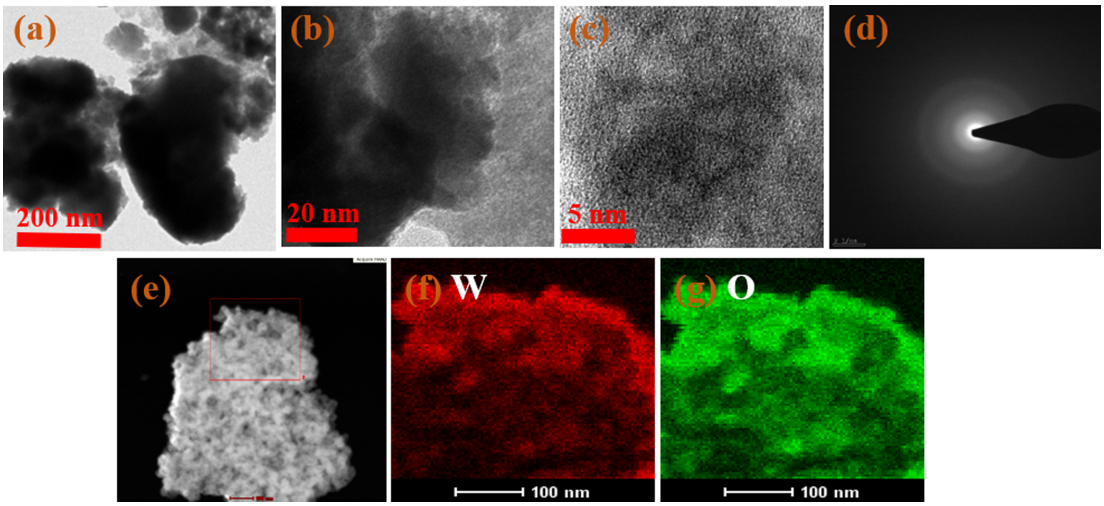

Fig. 2. (a, b) TEM images, (c) HR-TEM image, (d) SAED images, and (e–g) elemental mapping of We-WO_3 film.

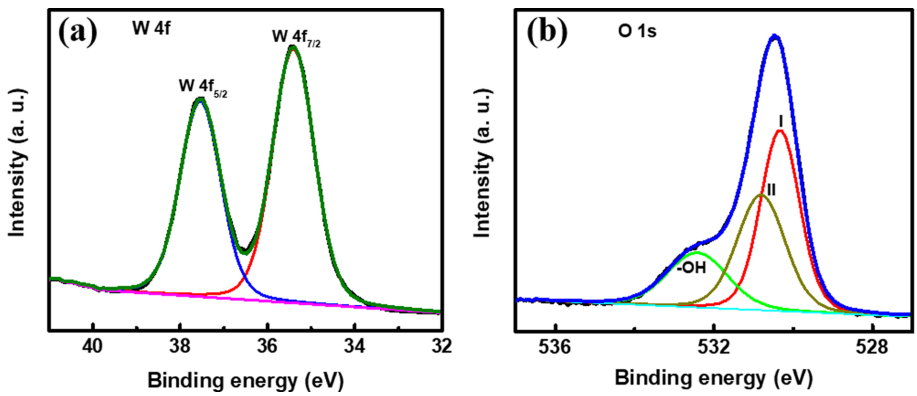

Fig. 3. XPS analysis: (a) W 4f and (b) O 1s spectra of We-WO_3 thin film.

The surface structure of the We-WO_3 thin film was thoroughly investigated using low-magnification TEM, HR-TEM, SAED, and elemental mapping measurements, as depicted in Fig. 2. The TEM image (Fig. 2(a)) reveals distinctive flaky nanostructures, providing detailed insights into the morphology of the thin film.

In contrast, the HRTEM images (Fig. 2(b, c)) exhibited an amorphous surface. Additionally, the SAED image of the We-WO_3 thin film (Fig. 2(d)) exhibited completely diffused, broad, and wide rings, strongly suggesting the amorphous nature of We-WO_3. Elemental mapping of the We-WO_3 film demonstrated that W and O were evenly distributed across the surface (Fig. 2(d–f)).

XRD was utilized to investigate the crystalline properties of the deposited WO_3 and We-WO_3 nanostructures (Fig. S3). The characteristic peaks at 30.5°, 35.4°, 51°, and 60.5° originate from the ITO substrate. Notably, no additional peaks were observed in the XRD patterns of the WO_3 and We-WO_3 film surfaces. The absence of peaks can be attributed to the amorphous nature and thin nanostructure of the films.[4,23)]

XPS was used to determine the chemical composition and valence states of the metal ions in We-WO_3 (Fig. 3). The survey analysis of the We-WO_3 film revealed an atomic composition of 17.1% W

and 82.9% O (Fig. S4(a)). The defined peaks at binding energies of 35.4 and 37.7 eV correspond to W $4f_{7/2}$ and W $4f_{5/2}$, respectively, indicating the +6-oxidation state (Fig. 3(a)). Furthermore, the XPS O1s spectra exhibited two major peaks at 530.4 and 530.8 eV, arising from the different chemical environments of the oxygen bonds in We-WO_3, denoted by I and II.[8,11] Additionally, a prominent peak appeared at 532.4 eV owing to the hydrophilic -OH group present on the We-WO_3 surface (Fig. 3(b)). This suggests that extended ultrasonication did not affect the binding energies of the W ions. However, ultrasonication may have enhanced the water enrichment of the surface of We-WO_3. The formation of water-enriched nanostructures is beneficial for improving the intercalation/deintercalation of Li^+ ions over the film surface, leading to improvements in the primary EC properties, such as optical modulation and switching speed.

TGA measurements were performed to verify the water enrichment of the surface of We-WO_3 after extended ultrasonication (Fig. 4). The WO_3 and We-WO_3 nanostructures exhibited an initial water loss up to 200 °C; this water was likely absorbed from the external environment. The mass loss in the temperature region of 200–300 °C may be associated with the strongly bonded water molecules on the surface of the nanostructure.[15,16]

In this region, We-WO_3 exhibited a significant loss of water molecules (approximately 17%), confirming the enhancement of its hydrophilic nature or water-enriched surface. FTIR measurements of We-WO_3 also revealed the introduction of hydrophilic groups, indicated by the appearance of a broad band in the wavelength range of 3000–3700 /cm (Fig. S4(b)) due to the O–H stretching vibration of the adsorbed water.[16]

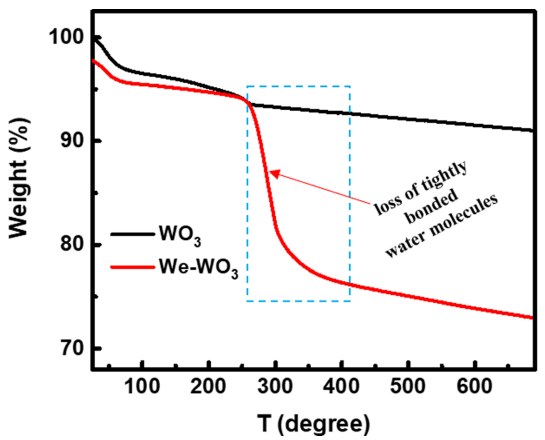

Fig. 4. TGA analysis of WO_3 and We-WO_3 thin films.

3.2 Electrochemical and optical characteristics

Cyclic voltammetry analysis of the WO_3 and We-WO_3 thin films was conducted in a non-aqueous solution of 1 M $LiClO_4$/PC. The experiment covered the potential range of -1 V to +1 V, with a scan rate of 50 mV/s. The results presented in Fig. 5(a) indicate that the redox peaks for We-WO_3 were more prominent, accompanied by higher current levels, compared with those of the WO_3 film electrode. This suggests that the water-enriched

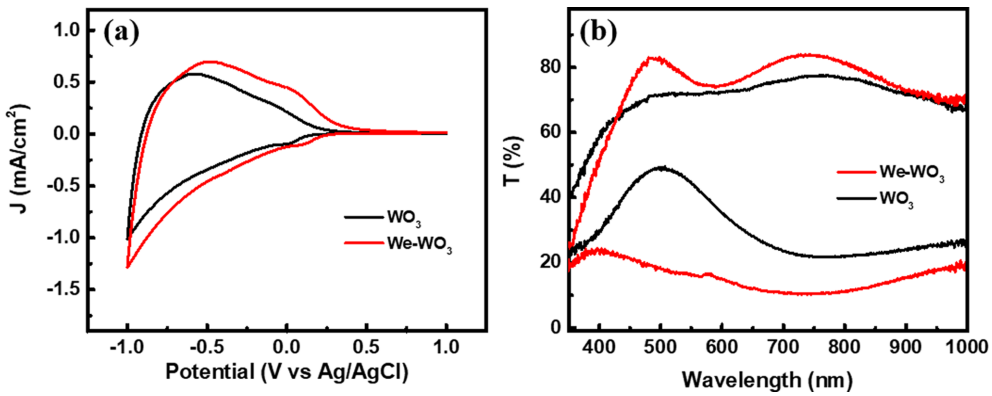

Fig. 5. (a) Cyclic voltammetry and (b) optical modulation data for WO_3 and We-WO_3 thin films.

nanostructure of We-WO_3 resulting from intense ultrasonication enhanced the transfer of Li^+ ions across the surface of the film. Upon optical examination, We-WO_3 exhibited exceptional optical contrast (%ΔT) of 73.6% at 750 nm (Fig. 5(b)).

In contrast, the WO_3 film displayed a %ΔT of only 56.7% at the same wavelength. A comprehensive summary of these results is presented in Table S1. The remarkable optical contrast achieved for the We-WO_3 films may be attributed to the larger exposed area and the deagglomerated morphology of the nanostructures. This morphology resulted from extended ultrasonication, which facilitated easy access of Li^+ ions across the surface.

Nyquist plots of both films were obtained by impedance measurements (Fig. S5). Notably, We-WO_3 demonstrated a charge-transfer resistance (R_{ct}) and series resistance (R_s) of 20.5 Ω and 7.5 Ω, respectively. In contrast, the WO_3 film electrode exhibited an R_{ct} of 25.3 Ω and R_s of 8.4 Ω. A comprehensive summary of these results is presented in Table S1. The favorable electrochemical performance of We-WO_3 was underscored by its significantly lower R_{ct}, which contributed to its improved charge transfer. In addition, the minimal S value can be attributed to the enhanced active surface area resulting from the dispersed and exposed morphologies, as evidenced by the SEM images. A larger surface area generally leads to lower resistance owing to improved electron flow, reduced congestion, and enhanced contact between materials. To further validate the augmented active surface area of We-WO_3, cyclic voltammetry measurements were conducted in 0.1 M $[Fe(CN)]^{3-}$ (Fig. S6). The electrochemically active surface area (EASA) was calculated using the Randles-Sevcik equation [4,26–28]. The We-WO_3 film electrode exhibited a large EASA (0.0021 cm^2) and a minimum peak separation (ΔE) of 0.25 V during the oxidation–reduction process, whereas WO_3 displayed a lower EASA (0.0014 cm^2) and ΔE of 0.30 V. The combination of the lowest R_{ct} and enhanced EASA for We-WO_3 is attributed to its dispersed morphology, which increases the number of active sites across the surface.

For optical characterization, the switching performance of WO_3 and We-WO_3 as EC films was investigated at 750 nm (Fig. 6(a)).

Amperometry was employed to monitor both films at a switching potential of ±1 V, and the corresponding bleaching time (t_b) and coloration time (t_c) were calculated. Here, t_c and t_b represent the times required to achieve 90% optical contrast in both states. The We-WO_3 EC film exhibited minimal t_c and t_b values of 3.3 s and 1.6 s, respectively. In contrast, the WO_3 EC film had t_c and t_b values of 5.2 s and 3.4 s, respectively, as summarized in Table S2. The current density curves (Fig. 6(b)), showing the switching performance, indicate that the We-WO_3 film exhibited higher current densities in both the oxidation and reduction processes than the WO_3 film. This observation further con-

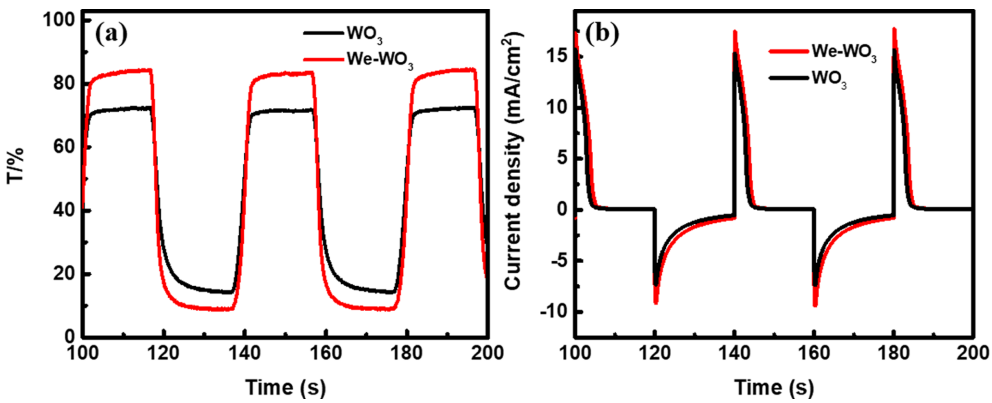

Fig. 6. (a) Switching performance of both thin films as ECDs and (b) corresponding current density curves for WO_3 and We-WO_3, measured at a switching potential of ±1 V.

firmed the efficient transfer of Li^+ ions over the water-enriched surface of the We-WO_3 film during the intercalation and deintercalation processes.

The coloration efficiency (CE), a crucial parameter for characterizing EC materials, was calculated using the following straightforward equation[8,11]:

$$CE = \Delta OD/(Q/A) = \log(Tb/Tc)/(Q/A)$$

where ΔOD is the optical density, Q is the charge capacity, A is the effective area, and T_b and T_c represent the transmittance of the films in their bleached and colored states, respectively. The efficiency was calculated by plotting the OD as a function of the charge density (C) for both films.

This result indicates that the EC film of We-WO_3 exhibited a higher CE value of 93.1 cm^2/C, whereas the CE of the WO_3 film was only 75.3 cm^2/C (Fig. 7(a)). Furthermore, the optical stability of both films was investigated at 750 nm over 1000 s, as depicted in Fig. 7(b).

When the films were used as ECDs, a nearly identical negligible degradation in $\%\Delta T$, i.e., only 1.9% over the applied period, was observed for both films. The overall enhanced EC performance of the We-WO_3 film can be attributed to the improved reactivity resulting from the refined morphology achieved by intense ultrasonication.

In addition to its remarkable EC performance, this study investigated the capacitive performance of We-WO_3 as an energy-storage electrode. Galvanostatic charge–discharge (GCD) curves of both film electrodes were acquired at various current densities (0.5–5 mA/cm^2) in 1.0 M $LiClO_4$/PC (Fig. 8(a, b)).

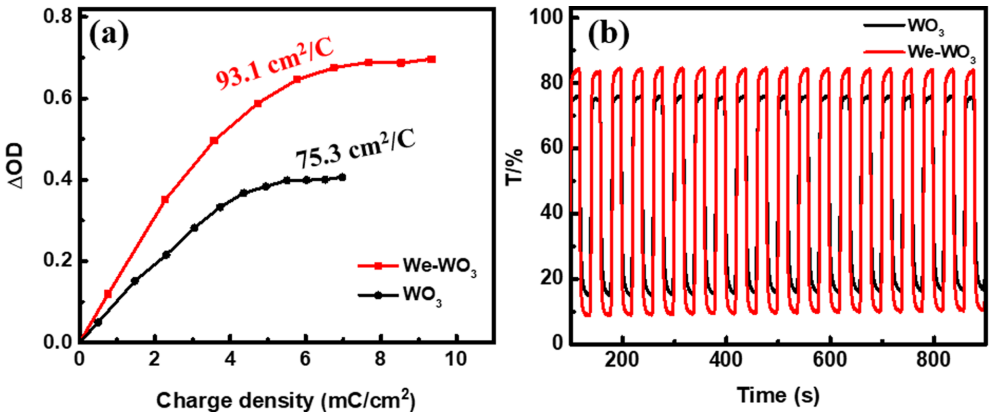

Fig. 7. (a) Coloration efficiency curves and (b) optical stability measurement for WO_3 and We-WO_3 ECDs.

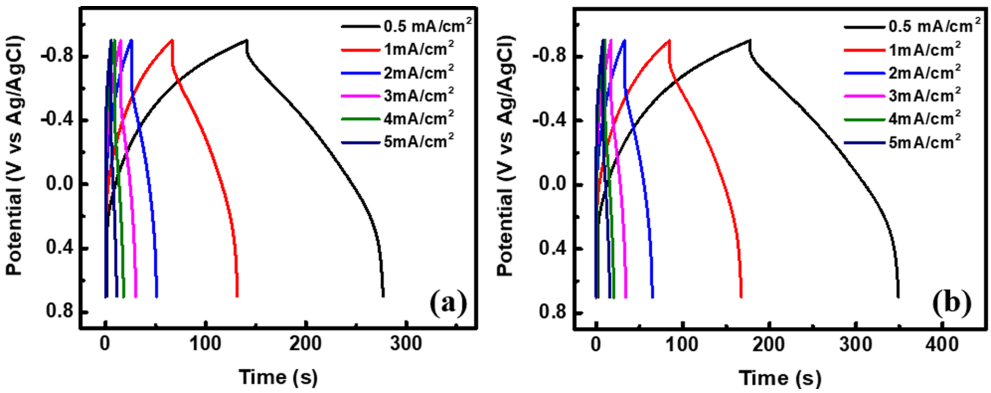

Fig. 8. GCD curves of (a) WO_3 and (b) We-WO_3 thin-film electrodes at various current densities.

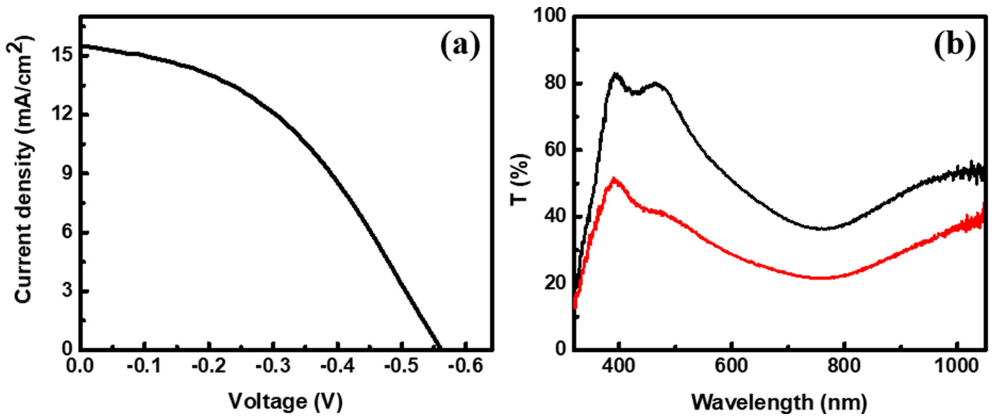

Fig. 9. (a) Photocurrent–voltage (*P–V*) curve for the QDSSC device under 1-sun illumination and (b) optical modulation measurement of We-WO_3 assisted by QDSSC in the absence of external power.

Notably, We-WO_3 demonstrated a peak areal capacitance (C_a) of 35.6 mF/cm^2 at a current density of 0.5 mA/cm^2, surpassing that of WO_3 (C_a = 28.1 mF/cm^2). The capacitance retention (%) and coulombic efficiency (%) of both film electrodes were also computed after 2,000 charge–discharge cycles at a current density of 5 mA/cm^2 within the potential range of -0.9–0.7 V. We-WO_3 demonstrated an optimal capacitance retention of 78.4% (Fig. S7(a)), indicating satisfactory cyclic performance, whereas WO_3 exhibited a competitive capacitive retention of 72.2% (Fig. S7(b)). Additionally, the coulombic efficiency of both films exceeded 95% in the measured GCD cycles. Consequently, the overall enhanced energy storage performance of We-WO_3 can be attributed to its acquired morphology, which features a high EASA and excellent reactivity for the efficient transfer of Li^+ ions.

The EC performance of We-WO_3 as part of an EC device without external wiring or a direct power supply was assessed by integrating it with an alternate power source. In this context, the previously prepared QDSSC served as an alternative power source. Cu_2S and FTO/TiO_2/CdS/CdSe/ZnO were used as the counter electrode and photoanode, respectively, for the QDSSC. Prior to its integration with the EC film of We-WO_3, the *J–V* performance of the QDSSC was evaluated under 1-sun illumination (Fig. 9(a)). This assessment yielded an optimal open-circuit voltage of 0.56 V, a current density of 15.6 mAcm^{-2}, and a fill factor of 42.4.

To observe the EC performance of the We-WO_3 film, an integrated device was assembled in a novel configuration, wherein the QDSSC and We-WO_3 EC films were fabricated with a Cu_2S counter electrode and a TiO_2 ionic layer, respectively, on the same substrate surface, as shown in Fig. S1. When the QDSSC was used as the power source, the We-WO_3 film exhibited coloration and bleaching, as confirmed by transmittance measurements. When assisted in the integrated device, the We-WO_3 film demonstrated a %ΔT of 26 at 750 nm (Fig. 9(b)). During the operation, the actual voltage delivered to the EC film may have been lower due to internal resistive losses and the current flow between QDSSC and EC device. The lower effective voltage might not have been sufficient to fully drive the electrochemical process in the We-WO_3 film. Therefore, power mismatch between EC device and QDSSC source plays a significant role in optimizing the performance of the integrated device.

4. Conclusions

A We-WO_3 film was synthesized using an extended, intense ultrasonication process, followed by a straightforward electrodeposition technique. The applicability of the film to both EC and energy storage devices was investigated. In terms of its role as an EC film, We-WO_3 exhibited an out-

standing optical modulation of 73.6%, a short coloration time of 3.3 s, and a coloration efficiency of 93.1 cm^2/C, with a reasonable areal capacitance of 35.6 mF/cm^2 and excellent capacitance retention. The enhanced performance of We-WO_3 can be predominantly attributed to the formation of a water-enriched nanostructure, which significantly increased the active surface area and improved the charge-transfer kinetics. A novel integrated device assembly was introduced to further extend the application scope. The assembly comprised a QDSSC as the power source to drive the EC performance of the We-WO_3 film without requiring an external power supply. The induced open-circuit voltage from the QDSSC source successfully enhanced the EC performance of the We-WO_3 film.

Acknowledgments

This research was supported by the Basic Science Research Program through the National Research Foundation of Korea (NRF), funded by the Ministry of Education [grant number 2018R1D1A3B05042787]. This work was also supported by the "Human Resources Program in Energy Technology" of the Korea Institute of Energy Technology Evaluation and Planning (KETEP) and was granted financial resources from the Ministry of Trade, Industry, and Energy, Republic of Korea [grant number 20204010600100].

Author contributions

Aryal Krishna Prasad: Conceptualization, investigation, writing – original draft

Kwang-Soon Ahn: Conceptualization, investigation, writing – review & editing, supervision, funding acquisition.

References

1. G. F. Cai, D. Zhou, Q. Q. Xiong, J. H. Zhang, X. L. Wang, C. D. Gu, and J. P. Tu, Efficient electrochromic materials based on TiO_2@WO_3 core/shell nanorod arrays, *Sol. Energy Mater. Sol. Cells*, **117**, 231–238 (2013).
2. J. M. O-Rueda de Leon, D. R. Acosta, U. Pal, and L. Castaneda, Improving electrochromic behavior of spray pyrolyzed WO_3 thin solid films by Mo doping, *Electrochim. Acta*, **56**, 2599–2605 (2011).
3. L. Wang, M. Guo, J. Zhan, X. Jiao, D. Chen, and T. Wang, A new design of an electrochromic energy storage device with high capacity, long cycle lifetime and multicolor display, *J. Mater. Chem. A*, **8**, 17098–17105 (2020).
4. A. K. Prasad, J.-Y. Park, H. Y. Jung, J. W. Kang, S.-H. Kang, and K. S. Ahn, Electrochemical deposition of Ni-WO_3 thin-film composites for electrochromic energy storage applications: Novel approach toward quantum-dot-sensitized solar cell-assisted Ni-WO_3 electrochromic device, *J. Ind. Eng. Chem.*, **117**, 500–509 (2023).
5. C. Fu, C. Foo, and P. S. Lee, One-step facile electrochemical preparation of WO_3/graphene nanocomposites with improved electrochromic properties, *Electrochim. Acta*, **117**, 139–144 (2014).
6. E. Vijayakumar, Y.-H. Yun, V. H. V. Quy, Y.-H. Lee, S.-H. Kang, K.-S. Ahn, and S. W. Lee, Development of tungsten trioxide using pulse and continuous electrodeposition and its properties in electrochromic devices, *J. Electrochem. Soc.*, **166**, D86–D92 (2019).
7. A. Khan, N. Y. Bhosale, S. S. Mali, C. K. Hong, and A. V. Kadam, Reduced graphene oxide layered WO_3 thin film with enhanced electrochromic properties, *J. Colloid Interface Sci.*, **571**, 185–193 (2020).
8. V. H. V. Quy, I.-R. Jo, S.-H. Kang, and K.-S. Ahn, Amorphous crystalline dual phase WO_3 synthesized by pulse-voltage electrodeposition and its application to electrochromic devices, *J. Ind. Eng. Chem.*, **94**, 264–271 (2020).
9. P.-W. Chen, C.-T. Chang, T.-F. Ko, S.-C. Hsu, K.-D. Li, and J.-Y. Wu, Fast response of complementary electrochromic device based on WO_3/NiO electrodes, *Sci. Rep.*, **10**, 8430 (2020).
10. M. R. Deylami, M. Javanbakht, H. Omidvar, K. Hooshyari, P. Salarizadeh, and M. B. Askari, Nickel-doped monoclinic WO_3 as high-performance anode material for rechargeable lithium ion battery, *J. Electroanal. Chem.*, **894**, 115383 (2021).
11. K. P. Aryal, J.-Y. Park, S.-H. Kang, and K. S. Ahn, Electrochemically co-deposited WO_3-V_2O_5 composites for electrochromic energy storage applications, *Electrochim. Acta*, **422**, 140340 (2022).
12. D. Zhou, F. Shi, D. Xie, D. H. Wang, X. H. Xia, X. L. Wang, C. D. Gu, and J. P. Tu, Bi-functional Mo-doped WO_3 nanowire array electrochromism-plus electrochemical energy storage, *J. Colloid Interface Sci.*, **465**, 112–120 (2015).
13. S. S. Kalanur and H. Seo, Influence of molybdenum doping on the structure, optical and electronic properties of WO_3 for improved solar water splitting, *J. Colloid Interface Sci.*, **509**, 440–447 (2018).
14. S. Xie, Z. Bi, Y. Chen, X. He, X. Guo, X. Gao, and X. Li, Electrodeposited Mo-doped WO_3 film with large optical modulation and high areal capacitance toward electrochromic energy-storage applications, *Appl. Surf. Sci.*, **459**, 774–781 (2018).
15. W. Cheng, E. Baudrin, B. Dunn, and J. I. Zink, Synthesis

and electrochromic properties of mesoporous tungsten oxide, *J. Mater. Chem.*, **11**, 92–97 (2001).
16. F. Liu, X. Chen, Q. Xia, L. Tian, and X. Chen, Ultrathin tungsten oxide nanowires: oleylamine assisted nonhydrolytic growth, oxygen vacancy and high photocatalytic properties, *RSC Adv.*, **5**, 77423–77428 (2015).
17. R. Azimirad, N. Naseri, O. Akhavan, and A. Z. Moshfegh, Hydrophilicity variation of WO_3 thin films with annealing temperature, *J. Phys. D: Appl. Phys.*, **40**, 1134–1137 (2007).
18. P. Judeinstein and J. Livage, Role of the water content on the electrochromic properties of WO_3, nH_2O thin films, *Mater. Sci. Eng. B*, **3(1–2)**, 129–132 (1989).
19. H. Ling, J. Wu, F. Su, Y. Tian, and Y. J. Liu, Automatic light-adjusting electrochromic device powered by perovskite solar cell, *Nat. Commun.*, **12**, 1010 (2021).
20. Y. Wang, L. Zhang, K. Cui, C. Xu, H. Li, H. Liu, and J. Yu, Solar driven electrochromic photoelectrochemical fuel cells for simultaneous energy conversion, storage and self-powered sensing, *Nanoscale*, **10**, 3421–3428 (2018).
21. K.-S. Ahn, S. J. Yoo, M.-S. Kang, J.-W. Lee, and Y.-E. Sung, Tandem dye-sensitized solar cell-powered electrochromic devices for the photovoltaic-powered smart window, *J. Power Sources*, **168(2)**, 533–536 (2007).
22. A. K. Prasad, I.-R. Jo, S.-H. Kang, and K.-S. Ahn, Novel method for synthesis of reduced graphene oxide–Cu_2S and its application as a counter electrode in quantum-dot-sensitized solar cells, *Appl. Surf. Sci.*, **564**, 150393 (2021).
23. I.-R. Jo, J. A. Rajesh, Y.-H. Lee, J.-H. Park, and K.-S. Ahn, Enhanced electrocatalytic activity and electrochemical stability of Cu_2S/PbS counter electrode for quantum-dot-sensitized solar cells, *Appl. Surf. Sci.*, **525**, 146643 (2020).
24. L. Jia, W. Ma, Q. Zhuang, Y. Zhang, and J. Dang, Controllable electrodeposition adjusts the electrochromic properties of Co and Mo co-modified WO_3 films, *Crystals*, **12(2)**, 190 (2022).
25. B.-R. Koo and H.-J. Ahn, Fast-switching electrochromic properties of mesoporous WO_3 films with oxygen vacancy defects, *Nanoscale*, **9**, 17788–17793 (2017).
26. B. Wang, W. Man, H. Yu, Y. Li, and F. Zheng, Fabrication of Mo-doped WO_3 nanorod arrays on FTO substrate with enhanced electrochromic properties, *Materials*, **11(9)**, 1627 (2018).
27. K. Z. Kamali, P. Alagarsamy, N. M. Huang, B. H. Ong, and H. N. Lim, Hematite nanoparticles-modified electrode based electrochemical sensing platform for dopamine, *Sci. World J.*, 396135 (2014).
28. H. Song, G. Xue, J. Zhang, G. Wang, B. Ye, S. Sun, L. Tian, Y. Li, Simultaneous voltammetric determination of dopamine and uric acid using carbon-encapsulated hollow Fe_3O_4 nanoparticles anchored to an electrode modified with nanosheets of reduced graphene oxide, *Microchim. Acta*, **184**, 843–853 (2017).